IEEE Robotics and Automation Letters (RA-L) paper, presented at ICRA 2024, Yokohama, Japan. Cite as RA-L paper.

Model-based Co-simulation of Flexible Mechanical Systems with Contacts Using Reduced Interface Models

Xu Dai[1], Ali Raoofian[1], József Kövecses[1] and Marek Teichmann[2]

***Abstract*—Co-simulation is a useful approach in the modelling of robotic systems composed of multiple parts. In co-simulation, the subsystems only exchange information at communication points. The time delay of information exchange may cause error and instability. Thus, an appropriate way to determine the interface variables between the communication points is essential for efficient and stable performance, especially for real-time applications. Reduced interface models (RIMs) can be used to represent the dynamic behaviour of the subsystems at the interface in co-simulation. Such a model-based co-simulation scheme was limited to systems consisting of rigid bodies in previous studies. In this work, we introduce the formulation of RIMs for flexible multibody systems and based on that propose a general co-simulation scheme for systems consisting of both rigid body components and elements with structural flexibility. A robotic model is employed as an example to demonstrate the co-simulation scheme, where a non-smooth subsystem with contact interactions is present. The advantages of constructing RIM using flexible mechanical system models over rigid body models are also addressed by comparing the effective mass properties and the simulation results.**

***Index Terms*—Dynamics, Flexible Robotics, Co-simulation, Reduced Interface Model, Contact Modelling**

I. Introduction

A general stable and efficient modelling and simulation approach is essential for robotic systems. A monolithic representation includes all components of the system in one single model [1], [2]. On the other hand, for more complicated systems consisting of multiple parts with different physical properties, co-simulation can provide an appropriate alternative, where each subsystem is modelled separately and different methods and time discretization may be employed. Co-simulation shows advantages in many applications [3], [4]. In robotic applications, the robotic arms usually have well-established models using joint angles to represent the configuration. The robotic arm is typically connected to another system, which involves contacts and can have different simulation requirements. In these applications, co-simulation is suitable to couple the robotic arm and the other system together.

The methods to establish the coupling between subsystems are critical to the performance and stability of co-simulation. In general, the subsystems only exchange information discretely at communication points. The time interval between two adjacent communication points is referred to as *macro time step*. During a macro time step, each subsystem is described by a set of dynamic equations and is numerically integrated with its own *micro time step*. The discretization and time delay in information exchange between subsystems can lead to inaccuracy and instability of the dynamic simulation [5].

To stabilize the co-simulation, different approaches have been proposed to approximate the interface variables inside the macro time step. The iterative methods are in general more stable [6] but not efficient enough for real-time applications. Our focus is on non-iterative methods for co-simulation, which have a broader range of applicability but are also more prone to stability problems.

Among the non-iterative coupling schemes, the so-called signal-based methods approximate the interface variables with extrapolation during the macro time step. Such approaches have limitations and are prone to inaccuracy and instability [7]. On the other hand, model-based methods take into account the system dynamics and determine the interface variables with system models. For example, model-based correctors can be added to extrapolations to reduce the error [8], [9].

The concept of the reduced interface model (RIM) has been introduced to model-based co-simulation recently, where reduced-order models are established to represent the dynamics associated with the interface and approximate the behaviour of the subsystems. The input/output at the interface is determined based on the simulation of these reduced models. RIMs contain the dynamic information of the subsystems and thus give a better approximation of the interface variables than extrapolations. Therefore, the RIM-based coupling shows more stable performance and accuracy than signal-based methods [3].

While the existing co-simulation methods, including the RIM-based approach, mostly focus on rigid multibody systems, many robotic models have to take into account struc-

Manuscript received: May, 26, 2023; Revised September, 20, 2023; Accepted November, 6, 2023.

This paper was recommended for publication by Editor Lucia Pallottino upon evaluation of the Associate Editor and Reviewers' comments.

This work was supported by CM Labs Simulations, Inc., the Natural Sciences and Engineering Research Council of Canada (NSERC), and the Fonds de Recherche du Québec – Nature et Technologies (FRQNT).

[1]Xu Dai, Ali Raoofian and József Kövecses are with the Department of Mechanical Engineering and Centre for Intelligent Machines, McGill University, 845 Rue Sherbrooke O., H3A0C3 Montréal, Canada. xu.dai@mail.mcgill.ca, ali.raoofian@mail.mcgill.ca, jozsef.kovecses@mcgill.ca

[2]Marek Teichmann is with CM Labs Simulations, Inc, 645 Wellington, H3C 1T2, Montréal, Canada. marek@cm-labs.com

Digital Object Identifier (DOI): see top of this page.

IEEE Robotics and Automation Letters (RA-L) paper, presented at ICRA 2024, Yokohama, Japan. Cite as RA-L paper.

tural properties and deformation. For such dynamic models with flexibility, the functioning and performance of the co-simulation coupling methods need to be evaluated in detail. Some literature discussed the co-simulation of flexible systems using signal-based approaches. For example, a parallel simulation scheme for elastic multibody chains was proposed in [10]. Flexibility was also considered in [11] for a four-bar mechanism. Recent studies such as [12] proposed stabilization approaches for the co-simulation of flexible systems based on signal-based coupling. Since signal-based coupling methods have limitations in accuracy and stability, we seek a generic co-simulation scheme for flexible systems from a model-based point of view.

In this paper, we introduce the RIM formulation for flexible systems. Based on that, we propose a model-based co-simulation approach for robotic systems with structural components. An example of a robotic model performing a contact task is employed to illustrate the co-simulation scheme.

II. Reduced Interface Modelling for Flexible Mechanical Systems

The RIM-based method provides a systematic way to reduce dimensionality and represent mechanical subsystems at the co-simulation interface. The RIM has been applied to different rigid multibody systems in previous studies [3], [13], [14].

In this section, the RIM-based approach is generalized for robotic systems consisting of both rigid bodies and flexible structural components. A novel formulation of RIM of flexible systems is introduced, where stiffness and damping terms are included. The RIM for constrained multibody systems with flexibility is also introduced.

A. Reduced interface model formulation

The interface represents the interaction between the subsystems in co-simulation. It is often determined by separating the whole system at a body or a joint, whose kinematic properties are described by a set of interface variables. The relationship between the interface velocities and the generalized velocities of the full-order model can be written as

$$\mathbf{u}_i = \mathbf{A}_i \dot{\mathbf{q}} \tag{1}$$

where the subscript i represents interface, $\mathbf{u}_i$ is an $n_i \times 1$ array of interface velocities, $\dot{\mathbf{q}}$ is the $n \times 1$ array of the generalized velocities of the full-order model, $\mathbf{A}_i$ is the interface Jacobian matrix.

In applications such as robotic arms, the deformation of the structural components is usually small. Thus, the floating frame of reference formulation can be applied, which represents the motion of a flexible system as a combination of the rigid body motion and the deformation [15]. The generalized coordinates can thus be written as an $n \times 1$ array $\mathbf{q} = \begin{bmatrix}\mathbf{q}_r & \mathbf{q}_e\end{bmatrix}^T$, where $\mathbf{q}_r$ is an $n_r \times 1$ array representing the rigid body motion and $\mathbf{q}_e$ is an $n_e \times 1$ array describing the deformation. Joint angles are frequently used to describe rigid body motions in robotics and can be selected for the elements of $\mathbf{q}_r$. In such applications, the generalized velocities of the robotic system are the joint rates $\dot{\mathbf{q}}_r$, and the rates of the coordinates describing the flexibility $\dot{\mathbf{q}}_e$.

The forces $\mathbf{f}$ applied to such a robotic system include the interface force $\mathbf{f}_i$, and the remaining generalized forces $\mathbf{f}_r$, which can be further decomposed to generalized elastic forces $\mathbf{f}_e$, generalized damping forces $\mathbf{f}_d$, and other generalized applied forces $\mathbf{f}_o$. The generalized elastic and damping forces are often written as $\mathbf{f}_e = -\mathbf{K}\mathbf{q}$ and $\mathbf{f}_d = -\mathbf{C}\dot{\mathbf{q}}$, where $\mathbf{K}$ is an $n \times n$ stiffness matrix, $\mathbf{C}$ is an $n \times n$ damping matrix. The other applied forces $\mathbf{f}_o$ also include the actuator torques/forces.

Therefore, the dynamic equations of the flexible robotic system can be written as

$$\begin{aligned}\begin{bmatrix}\mathbf{M}_{rr} & \mathbf{M}_{re}\\ \mathbf{M}_{er} & \mathbf{M}_{ee}\end{bmatrix}\begin{bmatrix}\ddot{\mathbf{q}}_r\\ \ddot{\mathbf{q}}_e\end{bmatrix} + \mathbf{c} = \mathbf{f}_i - \begin{bmatrix}\mathbf{0} & \mathbf{0}\\ \mathbf{0} & \mathbf{K}_{ee}\end{bmatrix}\begin{bmatrix}\mathbf{q}_r\\ \mathbf{q}_e\end{bmatrix}\\ - \begin{bmatrix}\mathbf{0} & \mathbf{0}\\ \mathbf{0} & \mathbf{C}_{ee}\end{bmatrix}\begin{bmatrix}\dot{\mathbf{q}}_r\\ \dot{\mathbf{q}}_e\end{bmatrix} + \mathbf{f}_o\end{aligned} \tag{2}$$

where the sub-blocks $\mathbf{M}_{rr}$, $\mathbf{M}_{re}$, $\mathbf{M}_{er}$, and $\mathbf{M}_{ee}$ form a $n \times n$ matrix $\mathbf{M}$, which is the mass matrix of the system; $\mathbf{c}$ is the Coriolis and centrifugal term, which is a function of $\mathbf{q}$ and $\dot{\mathbf{q}}$.

To re-parameterize the system considering the interface variables, a full coordinate transformation can be established for the velocity field as

$$\mathbf{u} = \begin{bmatrix}\mathbf{u}_i\\ \mathbf{u}_a\end{bmatrix} = \begin{bmatrix}\mathbf{A}_i\\ \mathbf{B}\end{bmatrix}\dot{\mathbf{q}} = \mathbf{J}\dot{\mathbf{q}} \tag{3}$$

where $\mathbf{u}$ is a new set of generalized velocities that includes the interface velocities and an $(n - n_i) \times 1$ array of the admissible velocities $\mathbf{u}_a$; $\mathbf{J}$ is a square Jacobian matrix. Correspondingly, the transformation of the generalized forces and momenta can be obtained as $\mathbf{J}^T\boldsymbol{\tau} = \mathbf{f}$ and $\mathbf{J}^T\mathbf{s} = \mathbf{p}$, where $\boldsymbol{\tau}$ and $\mathbf{s}$ represent the forces and momenta energetically conjugated to $\mathbf{u}$; $\mathbf{p}$ is the momenta conjugated to $\dot{\mathbf{q}}$. Specifically, for the generalized interface forces we can write

$$\mathbf{f}_i = \mathbf{J}^T\boldsymbol{\tau}_i = \mathbf{A}_i^T\boldsymbol{\lambda} \quad \text{and} \quad \boldsymbol{\tau}_i = \begin{bmatrix}\boldsymbol{\lambda}\\ \mathbf{0}\end{bmatrix} \tag{4}$$

where $\boldsymbol{\tau}_i$ is an $n \times 1$ array of the generalized interface forces energetically conjugated to $\mathbf{u}$, $\boldsymbol{\lambda}$ is an $n_i \times 1$ array of the generalized interface forces conjugated to $\mathbf{u}_i$.

We can transform the dynamic equations from the basis of $\dot{\mathbf{q}}$ to $\mathbf{u}$ using the *central variational equation* in the momentum basis as

$$\delta\mathbf{p}^T(\mathbf{M}^{-1}(\mathbf{f} - \mathbf{c}) - \ddot{\mathbf{q}}) = \delta\mathbf{s}^T\mathbf{J}(\mathbf{M}^{-1}(\mathbf{f} - \mathbf{c}) - \ddot{\mathbf{q}}) = 0 \tag{5}$$

The dynamic equation corresponding to $\mathbf{u}$ can be derived as

$$\begin{aligned}(\mathbf{J}\mathbf{M}^{-1}\mathbf{J}^T)^{-1}\dot{\mathbf{u}} + (\mathbf{J}\mathbf{M}^{-1}\mathbf{J}^T)^{-1}(\mathbf{J}\mathbf{M}^{-1}\mathbf{c} - \dot{\mathbf{J}}\dot{\mathbf{q}})\\ = \boldsymbol{\tau}_i + (\mathbf{J}\mathbf{M}^{-1}\mathbf{J}^T)^{-1}\mathbf{J}\mathbf{M}^{-1}\mathbf{f}_r\end{aligned} \tag{6}$$

Note that

$$\mathbf{J}\mathbf{M}^{-1}\mathbf{J}^T = \begin{bmatrix}\mathbf{A}_i\mathbf{M}^{-1}\mathbf{A}_i^T & \mathbf{A}_i\mathbf{M}^{-1}\mathbf{B}^T\\ \mathbf{B}\mathbf{M}^{-1}\mathbf{A}_i^T & \mathbf{B}\mathbf{M}^{-1}\mathbf{B}^T\end{bmatrix} \tag{7}$$

If the matrix $\mathbf{B}$ in Eq. (7) is defined to satisfy

$$\mathbf{A}_i\mathbf{M}^{-1}\mathbf{B}^T = \mathbf{0} \tag{8}$$

the off-diagonal blocks of $\mathbf{J}\mathbf{M}^{-1}\mathbf{J}^T$ are eliminated and two sets of velocities $\mathbf{u}_i$ and $\mathbf{u}_a$ are decoupled. The dynamic equations

IEEE Robotics and Automation Letters (RA-L) paper, presented at ICRA 2024, Yokohama, Japan. Cite as RA-L paper.

associated with the interface variables can then be extracted from Eq. (6) as

$$(\mathbf{A}_i\mathbf{M}^{-1}\mathbf{A}_i^T)^{-1}\dot{\mathbf{u}}_i + (\mathbf{A}_i\mathbf{M}^{-1}\mathbf{A}_i^T)^{-1}(\mathbf{A}_i\mathbf{M}^{-1}\mathbf{c} - \dot{\mathbf{A}}_i\dot{\mathbf{q}}) = \boldsymbol{\lambda} + (\mathbf{A}_i\mathbf{M}^{-1}\mathbf{A}_i^T)^{-1}\mathbf{A}_i\mathbf{M}^{-1}\mathbf{f}_r \quad (9)$$

which is the *reduced interface model* (RIM) for the subsystem.

In Eq. (9), the generalized elastic and damping forces are grouped in $\mathbf{f}_r$ together with other forces. One possibility is that the elastic and damping forces are considered constant during the macro time step. However, to better capture the state-dependence of the forces, the elastic and damping forces can also be formulated separately in the macro time step.

In Eq. (6), $\mathbf{J}$ is a full-rank square matrix and is invertible, thus $(\mathbf{J}\mathbf{M}^{-1}\mathbf{J}^T)^{-1}\mathbf{J}\mathbf{M}^{-1}\mathbf{f}_r = \mathbf{J}^{-T}\mathbf{f}_r$. Considering $\mathbf{J}^{-1} = \begin{bmatrix}\mathbf{D} & \mathbf{G}\end{bmatrix}$ where $\mathbf{D}$ is of size $n \times n_i$ and $\mathbf{G}$ is of size $n \times (n-n_i)$, for the damping forces we can write

$$\mathbf{J}^{-T}\mathbf{f}_d = -\mathbf{J}^{-T}\mathbf{C}\mathbf{J}^{-1}\mathbf{u} = -\begin{bmatrix}\mathbf{D}^T\mathbf{C}\mathbf{D} & \mathbf{D}^T\mathbf{C}\mathbf{G} \\ \mathbf{G}^T\mathbf{C}\mathbf{D} & \mathbf{G}^T\mathbf{C}\mathbf{G}\end{bmatrix}\begin{bmatrix}\mathbf{u}_i \\ \mathbf{u}_a\end{bmatrix} \quad (10)$$

The generalized damping forces are not decoupled by the $\mathbf{J}$ transformation. For the interface dynamics, we can write the effective damping forces as

$$\boldsymbol{\tau}_{di} = -\mathbf{D}^T\mathbf{C}\mathbf{D}\mathbf{u}_i - \mathbf{D}^T\mathbf{C}\mathbf{G}\mathbf{u}_a \quad (11)$$

where $\mathbf{D}^T\mathbf{C}\mathbf{D}$ can be seen as the *effective damping matrix* for the RIM and is denoted as $\mathbf{C}_{eff}$.

Similarly, the effective elastic force can be written as

$$\boldsymbol{\tau}_{ei} \simeq -\mathbf{D}^T\mathbf{K}\mathbf{D}\mathbf{d}_i - \mathbf{D}^T\mathbf{K}\mathbf{G}\mathbf{d}_a \quad (12)$$

where $\mathbf{d}_i$ and $\mathbf{d}_a$ are the position level coordinates related to $\mathbf{u}_i$ and $\mathbf{u}_a$, $\mathbf{D}^T\mathbf{K}\mathbf{D}$ can be considered as the *effective stiffness matrix* and is denoted as $\mathbf{K}_{eff}$.

Then Eq. (9) can be rewritten in a more compact form as

$$\mathbf{M}_{eff}\dot{\mathbf{u}}_i + \mathbf{z}_i = \boldsymbol{\lambda} + \boldsymbol{\lambda}_o - \mathbf{K}_{eff}\mathbf{d}_i - \mathbf{C}_{eff}\mathbf{u}_i \quad (13)$$

where

$$\mathbf{M}_{eff} = (\mathbf{A}_i\mathbf{M}^{-1}\mathbf{A}_i^T)^{-1} \quad (14)$$

is the $n_i \times n_i$ effective mass matrix;

$$\boldsymbol{\lambda}_o = (\mathbf{A}_i\mathbf{M}^{-1}\mathbf{A}_i^T)^{-1}\mathbf{A}_i\mathbf{M}^{-1}\mathbf{f}_o - \mathbf{D}^T\mathbf{C}\mathbf{G}\mathbf{u}_a - \mathbf{D}^T\mathbf{K}\mathbf{G}\mathbf{d}_a \quad (15)$$

represents the other effective forces excluding the state-dependent elastic and damping terms, and

$$\mathbf{z}_i = (\mathbf{A}_i\mathbf{M}^{-1}\mathbf{A}_i^T)^{-1}(\mathbf{A}_i\mathbf{M}^{-1}\mathbf{c} - \dot{\mathbf{A}}_i\dot{\mathbf{q}}) \quad (16)$$

is the non-linear inertia term.

In order to determine the effective stiffness and damping matrices, the $\mathbf{B}^T$ matrix that is an orthogonal complement to $\mathbf{A}_i\mathbf{M}^{-1}$ should be properly determined for the definition of $\mathbf{D}$ and $\mathbf{G}$. This matrix can be evaluated based on Eq. (8), but it is not unique. Assume that $\mathbf{B}_1$ and $\mathbf{B}_2$ are two possible solutions for (8), then $\mathbf{D}_1$, $\mathbf{G}_1$, $\mathbf{D}_2$ and $\mathbf{G}_2$ can be determined accordingly. From Eq. (8), the columns of $\mathbf{B}_1^T$ and $\mathbf{B}_2^T$ both span the null space of $\mathbf{A}_i\mathbf{M}^{-1}$. Thus, $\mathbf{B}_2 = \mathbf{T}\mathbf{B}_1$, where $\mathbf{T}$ is a full rank transformation matrix. It can be proven that $\mathbf{D}_2 = \mathbf{D}_1$ and $\mathbf{G}_2 = \mathbf{G}_1\mathbf{T}^{-1}$. It shows that different solutions to $\mathbf{B}$ lead to the same $\mathbf{K}_{eff}$ and $\mathbf{C}_{eff}$. Therefore, the formulation as Eq. (13) is uniquely determined once $\mathbf{A}_i$ is defined, no matter which $\mathbf{B}$ is selected.

Eq. (13) provides a general form for the RIM of flexible systems, in which the effective elastic and damping forces are state-dependent. The formulation in Eq. (13) has comparable computational efficiency as Eq. (9) while more accurately capturing the force terms in the macro time step. The RIM of systems with only rigid modes can be seen as a special case of Eq. (13), where the terms related to deformation coordinates do not exist.

B. Reduced interface model for constrained robotic systems

The elements of the system can be subjected to additional physical interactions that can be described by employing kinematic constraints. These constraints can be written at the velocity level as

$$\mathbf{w}_c = \begin{bmatrix}\mathbf{w}_b \\ \mathbf{w}_u\end{bmatrix} = \begin{bmatrix}\mathbf{A}_b \\ \mathbf{A}_u\end{bmatrix}\dot{\mathbf{q}} = \mathbf{A}_c\dot{\mathbf{q}} \quad (17)$$

where $\mathbf{w}_c$ represents the m constrained velocities and $\mathbf{A}_c$ is the constraint Jacobian matrix. The kinematic constraints are divided into bilateral and unilateral constraints, indicated by the subscript b and u, respectively. Typical examples include $\mathbf{w}_b = \mathbf{0}$ and $\mathbf{w}_u \geq \mathbf{0}$.

Particularly, the contact interactions in the system can be represented with unilateral constraints, where a set of complementarity conditions also needs to be considered between the constrained kinematic variables and the related constraint forces. For example, in the normal direction of the contact, to avoid penetration and tensile force, the complementarity condition at the acceleration level can be written in the form of

$$\mathbf{0} \leq \dot{\mathbf{w}}_n \perp \boldsymbol{\lambda}_n \geq \mathbf{0} \quad (18)$$

where $\dot{\mathbf{w}}_n$ is the relative acceleration in the normal direction of contact, $\boldsymbol{\lambda}_n$ is the normal contact force. Similarly, in the tangential plane of the contact, when the *box friction model* is used to describe friction, the Coulomb friction cone is approximated by a pyramid, and two orthogonal directions are used to describe the sliding. In such a model, the relationship between the friction force and the sliding motion can also be represented with complementarity conditions.

The dynamic equations, the kinematic constraints, and the complementarity conditions can then be written together to form a mixed linear complementarity problem (MLCP)

$$\begin{cases}\begin{bmatrix}\mathbf{M} & -\mathbf{A}_c^T \\ \mathbf{A}_c & \mathbf{0}\end{bmatrix}\begin{bmatrix}\ddot{\mathbf{q}} \\ \boldsymbol{\lambda}_c\end{bmatrix} + \begin{bmatrix}\mathbf{c} - \mathbf{f}_r - \mathbf{A}_i^T\boldsymbol{\lambda}_i \\ \dot{\mathbf{A}}_c\dot{\mathbf{q}}\end{bmatrix} = \begin{bmatrix}\mathbf{0} \\ \dot{\mathbf{w}}_c\end{bmatrix} \\ \dot{\mathbf{w}}_c \perp \boldsymbol{\lambda}_c \in [\boldsymbol{\lambda}_c^{\text{lo}}, \boldsymbol{\lambda}_c^{\text{up}}]\end{cases} \quad (19)$$

where the acceleration $\ddot{\mathbf{q}}$, $\dot{\mathbf{w}}_c$ and the constraint force $\boldsymbol{\lambda}_c$ are the unknowns to solve. For bilateral constraints, the upper bound $\boldsymbol{\lambda}_c^{\text{up}}$ is $+\infty$ and the lower bound $\boldsymbol{\lambda}_c^{\text{lo}}$ is $-\infty$; In the normal direction of contact, $\boldsymbol{\lambda}_c^{\text{up}}$ is $+\infty$ and $\boldsymbol{\lambda}_c^{\text{lo}} = \mathbf{0}$; the friction force in the jth contact $\lambda_{t,j}$ is bounded by $[-\mu\lambda_{n,j}, +\mu\lambda_{n,j}]$ according to Coulomb's friction law, where μ is the friction coefficient.

IEEE Robotics and Automation Letters (RA-L) paper, presented at ICRA 2024, Yokohama, Japan. Cite as RA-L paper.

The MLCP as Eq. (19) can be solved by various methods, e.g., direct pivoting techniques [16], where the elements of $\boldsymbol{\lambda}_c$ and $\dot{\mathbf{w}}_c$ fall in one of the two categories: active and tight, indicated by subscripts α and β, respectively. The active group includes bilateral constraints, the constraints in the normal direction of closed contacts, and static friction, which all ensure that $\dot{\mathbf{w}}_\alpha = \mathbf{0}$. The tight constraints include open contacts and sliding friction, where $\dot{\mathbf{w}}_\beta$ can be non-zero while $\boldsymbol{\lambda}_\beta$ is either at the lower or at the upper bound.

When constructing the RIM of such constrained flexible systems, a straightforward way is to assume that the state of constraints does not change during the macro time step, i.e., the active constraints remain active between communication points and the tight constraints remain tight. In this way, at the communication points, the constrained velocities can be regrouped as

$$\mathbf{w}_c = \begin{bmatrix} \mathbf{w}_\alpha \\ \mathbf{w}_\beta \end{bmatrix} = \begin{bmatrix} \mathbf{A}_\alpha \\ \mathbf{A}_\beta \end{bmatrix} \dot{\mathbf{q}} \tag{20}$$

The dynamic equations of RIM of flexible systems become

$$\hat{\mathbf{M}}_{eff}\dot{\mathbf{u}}_i + \hat{\mathbf{z}}_i = \boldsymbol{\lambda} + \hat{\boldsymbol{\lambda}}_o - \hat{\mathbf{K}}_{eff}\mathbf{d}_i - \hat{\mathbf{C}}_{eff}\mathbf{u}_i \tag{21}$$

where

$$\hat{\mathbf{M}}_{eff} = (\mathbf{A}_i\mathbf{P}_m\mathbf{M}^{-1}\mathbf{A}_i^T)^{-1} \tag{22}$$

$$\begin{aligned}\hat{\boldsymbol{\lambda}}_o =& \hat{\mathbf{M}}_{eff}[\mathbf{A}_i\mathbf{P}_m\mathbf{M}^{-1}(\mathbf{f}_o + \mathbf{f}_\beta - \mathbf{K}\mathbf{P}_\alpha\mathbf{q} - \mathbf{C}\mathbf{P}_\alpha\dot{\mathbf{q}})] \\ & - \mathbf{D}^{\mathrm{T}}\mathbf{P}_m^T\mathbf{K}\mathbf{P}_m\mathbf{G}\mathbf{d}_a - \mathbf{D}^{\mathrm{T}}\mathbf{P}_m^T\mathbf{C}\mathbf{P}_m\mathbf{G}\mathbf{u}_a\end{aligned} \tag{23}$$

$$\begin{aligned}\hat{\mathbf{z}}_i =& \hat{\mathbf{M}}_{eff}(\mathbf{A}_i\mathbf{P}_m\mathbf{M}^{-1}\mathbf{c} - \dot{\mathbf{A}}_i\dot{\mathbf{q}}) + \\ & \hat{\mathbf{M}}_{eff}[\mathbf{A}_i\mathbf{M}^{-1}\mathbf{A}_\alpha^T(\mathbf{A}_\alpha\mathbf{M}^{-1}\mathbf{A}_\alpha^T)^{-1}\dot{\mathbf{A}}_\alpha\dot{\mathbf{q}}]\end{aligned} \tag{24}$$

In Eq. (22)-(24), $\mathbf{P}_\alpha = \mathbf{M}^{-1}\mathbf{A}_\alpha^T(\mathbf{A}_\alpha\mathbf{M}^{-1}\mathbf{A}_\alpha^T)^{-1}\mathbf{A}_\alpha$ is the projector matrix onto the subspace of the active constraints; $\mathbf{P}_m = \mathbf{I} - \mathbf{P}_\alpha$. The term $\mathbf{f}_\beta = \mathbf{A}_\beta^T\boldsymbol{\lambda}_\beta$ is known after solving Eq. (19) for the full model at the communication points and is considered constant inside the macro time step. In Eq. (21), the modified effective stiffness and damping matrices are $\hat{\mathbf{K}}_{eff} = \mathbf{D}^{\mathrm{T}}\mathbf{P}_m^T\mathbf{K}\mathbf{P}_m\mathbf{D}$ and $\hat{\mathbf{C}}_{eff} = \mathbf{D}^{\mathrm{T}}\mathbf{P}_m^T\mathbf{C}\mathbf{P}_m\mathbf{D}$, which retain the important mathematical properties of $\mathbf{K}$ and $\mathbf{C}$ such as being symmetric and positive semi-definite.

Eq. (21) provides a systematic approach to constructing the RIMs of constrained flexible systems. When the system is unconstrained, $\mathbf{P}_\alpha$ and $\mathbf{A}_\alpha$ vanish, and the formulation in Eqs. (22)-(24) becomes equivalent to the one in Eqs. (14)-(16). Thus, the dynamic equation in (13) can be seen as a special case of Eq. (21).

III. Co-simulation Model

The RIM-based co-simulation is suitable for applications such as the simulation of robotic contact tasks. We illustrate it here with a space robotic example, where the robotic arm and an end-effector attached to it are simulated with different time rates.

A. Co-simulation setup

The structure of the co-simulated model is shown in Fig. 1. The system is divided into two parts. The first subsystem is the robotic arm and the second subsystem is the end-effector with its interaction with a static wall. The end-effector is connected to the last link (Link 7) of the robotic arm. In this model, co-simulation is applied because of the nature of the system. The robotic arm model is usually pre-established, using joint angles to describe its configuration. The end-effector subsystem, on the other hand, can have various contact modes during tasks such as pushing, grasping, and inserting, leading to different requirements and formulations for contact simulation. It is often modelled with a set of dependent coordinates together with constraints, which is different from the robotic arm model. Therefore, it is natural to model the two subsystems separately and couple them together, which brings out the necessity of co-simulation.

The end-effector subsystem can vary in different tasks. In this paper, we focus more on analyzing the properties of the RIM of the robotic arm. Therefore, the end-effector is simplified as one claw-shaped connector of 50kg fixed to the robotic arm as shown in Fig. 1. The RIM of the end-effector together with contacts is formulated following Eq. (21)-(24). A more detailed study on different formulations of contact problems in RIM-based co-simulation can be found in [13].

The interface between the robotic arm and the end-effector is defined by cutting Link 7 at its centre of mass. This results in two interface reference frames at the location of separation for the two subsystems. For both subsystems, the interface velocity $\mathbf{u}_i$ has six degrees of freedom and consists of the translational velocity of the interface reference point and the angular velocity of the interface frame.

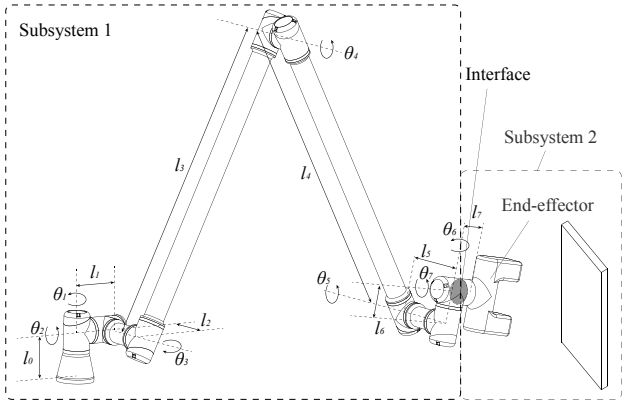

Fig. 1. Structure of the co-simulated model consisting of the robotic arm and the end-effector subsystem.

Fig. 2 shows the co-simulation scheme between the robotic arm and the end-effector subsystem. Between two adjacent communication points, the two subsystems are simulated and integrated separately without the exchange of information. A RIM is created for each subsystem based on Eq. (21). It is simulated with the other subsystem during the macro time step, as indicated by the solid arrows. The RIMs are only updated at each communication point based on the current status of the corresponding subsystems, as indicated by the dash arrows. Semi-implicit Euler method is employed as the integration method inside the macro time step.

IEEE Robotics and Automation Letters (RA-L) paper, presented at ICRA 2024, Yokohama, Japan. Cite as RA-L paper.

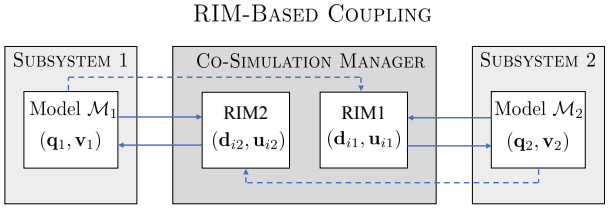

Fig. 2. The coupling scheme of the RIM-based co-simulation between two mechanical subsystems [14].

When the RIM-subsystem pair is simulated within the macro time step, the two interface reference frames for the two subsystems should stay together, which can be achieved by adding kinematic constraints at the interface. Specifically, we denote the robotic arm subsystem as $\mathcal{M}_1$ and the RIM of the end-effector subsystem as RIM2. When $\mathcal{M}_1$ and RIM2 are simulated together, besides their dynamic equations, the kinematic constraints at the interface should also hold, which can be written in the velocity level as $\mathbf{A}_{i,\mathcal{M}_1}\mathbf{v}_{\mathcal{M}_1} - \mathbf{u}_{i,RIM2} = \mathbf{0}$. Similarly, constraints should be added for the other RIM-subsystem pair as $\mathbf{A}_{i,\mathcal{M}_2}\mathbf{v}_{\mathcal{M}_2} - \mathbf{u}_{i,RIM1} = \mathbf{0}$.

B. The robotic arm model

The robotic arm model used in this work has a symmetric structure and has seven revolute joints.

To compare the properties of RIMs between the rigid and flexible systems, two robotic arm models are developed. In the first model, all links are considered as rigid bodies. The second model is flexible by taking into account the structural components. Specifically, in the flexible model, the two long links are considered flexible and are modelled as Euler-Bernoulli beams. The other links are modelled as rigid bodies because the influence of their deformation is negligible compared to the long booms. For each flexible boom, the bending deformation in each perpendicular plane is represented by two eigenmodes of the clamped-free boundary value problem. Therefore, the deformation of the system is described by eight coordinates while the rigid body motion is represented by the seven joint angles. Hence, the flexible model has fifteen degrees of freedom in total while the rigid model has seven degrees of freedom.

For both models, the links are simplified as cylinders. The material of the robot arm is assumed to be aluminum, with a density of $\rho = 2700 kg/m^3$. In the flexible model, the modulus of elasticity of the two long links is $E = 6.9 \times 10^{10} Pa$. The diameters of the cross-section of all links are set as $0.3m$. The parameters of each link of the robot arm are listed in Table I.

TABLE I
GEOMETRIC AND PHYSICAL PARAMETERS OF THE ROBOTIC ARM MODEL.

Link Index	Length (m)	Mass (kg)	E (GPa)
0, 7	0.38	72.5	-
1, 6	0.64	121.2	-
2, 5	0.50	96.2	-
3, 4	6.85	1307.3	- or 69

IV. Results and Discussion

The aforementioned rigid and flexible robotic models have an essential difference in their physical properties, i.e., taking into account deformation or not. Both the rigid and flexible robotic models can be co-simulated with the end-effector subsystem through RIM-based coupling. In the co-simulation, the RIMs constructed based on the rigid and flexible robotic arm models are referred to as *rigid RIM* and *flexible RIM* respectively in the following sections. Here we compare the properties of the rigid and flexible RIMs and show how the difference can affect the numerical performance in the co-simulation.

A. Comparison between flexible and rigid RIM representations

In this section, we illustrate the comparison between the rigid RIM and the flexible RIM. For both rigid and flexible robotic arm models, the interface is defined at the centre of mass of Link 7, and the RIMs have six degrees of freedom. However, the two RIM representations have different properties.

An important difference relates to the effective mass matrices. The effective mass matrix can be evaluated at a given configuration of the robotic arm as Eq. (14) or (22). Once the mass matrix is determined, it can also be used to determine any effective mass or effective moment of inertia associated with any direction in three-dimensional physical space. For example, considering all possible directions of translational motion in the task space, the effective mass values geometrically form a belted ellipsoid [17] associated with a configuration of the system. This ellipsoid indicates the effective mass properties in the task space at the interface. In general, a more elongated shape of the ellipsoid represents a more ill-conditioned effective mass matrix, which can be more prone to numerical problems in simulation.

A group of representative configurations of the robotic arm is selected to compare the effective mass between the rigid and the flexible RIMs (See Fig. 3-5). Fig. 3b shows the effective mass ellipsoid associated with both the flexible and rigid RIMs in Configuration A. It can be seen that for any given direction, the magnitude of the effective mass of the rigid RIM is larger than or equal to the effective mass obtained for the flexible RIM. The shape of the ellipsoid for the rigid RIM is typically more elongated than that for the flexible RIM. This is an indication that including structural flexibility in the model can improve the conditioning of the mass matrix.

Analysis of the effective mass for other configurations gives similar results, as shown in Fig. 4-5. Note that in Configuration C, the long booms of the robotic arm are stretched out and aligned (See Fig. 5a). In this posture, the arm is naturally in a near-singular configuration. According to the effective mass ellipsoids in Fig. 5b, the difference between the flexible RIM and the rigid RIM is more significant than in other configurations.

The properties of the effective mass matrix are also indicated by its condition number. Though the condition number

IEEE Robotics and Automation Letters (RA-L) paper, presented at ICRA 2024, Yokohama, Japan. Cite as RA-L paper.

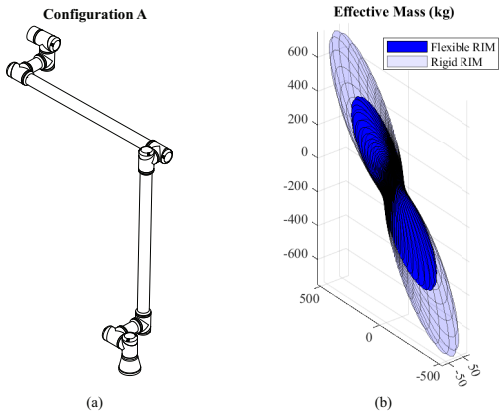

Fig. 3. (a) The robotic arm in Configuration A. (b) The belted-ellipsoid shapes of the effective mass matrix in Configuration A.

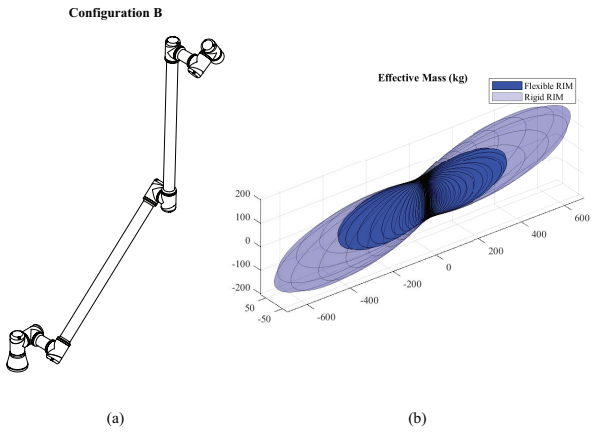

Fig. 4. (a) The robotic arm in Configuration B. (b) The belted-ellipsoid shapes of the effective mass matrix in Configuration B.

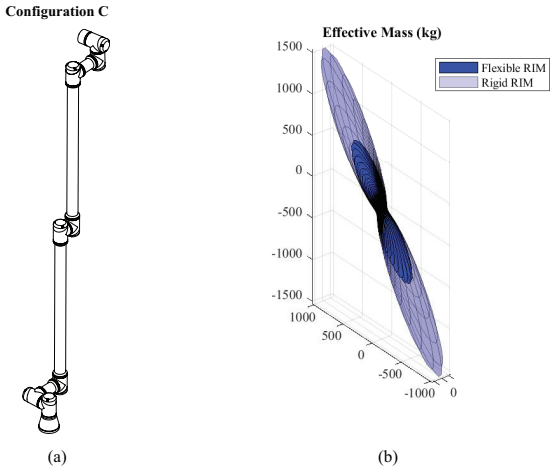

Fig. 5. (a) The robotic arm in Configuration C. (b) The belted-ellipsoid shapes of the effective mass matrix in Configuration C.

TABLE II
CONDITION NUMBER OF THE EFFECTIVE MASS MATRIX IN DIFFERENT CONFIGURATIONS.

Configuration	A	B	C
Flexible RIM	2.59×10^3	2.88×10^3	3.88×10^3
Rigid RIM	3.41×10^3	5.39×10^3	4.89×10^5
Flexible RIM (θ_1, θ_2 fixed)	2.65×10^3	3.30×10^3	2.18×10^4
Rigid RIM (θ_1, θ_2 fixed)	2.66×10^{17}	3.86×10^{16}	1.33×10^{21}

depends on physical units and thus does not have direct physical meaning, it can still reflect the numerical performance in the simulation. Extremely large condition numbers are a typical sign of ill-conditioned matrices, which are more prone to large numerical errors. The condition numbers of the effective mass matrices of the rigid and flexible RIMs for each configuration are listed in Table II. To introduce a more challenging case, we can lock certain joints in these configurations with bilateral constraints, which reduces the number of degrees of freedom of the model. In this case, the effective mass matrix is determined based on Eq. (22). Specifically, here the two joints represented by the joint angles θ_1 and θ_2 in Fig. 1 are locked to compare the condition of the mass matrices between the rigid and the flexible RIMs. In table II, the first and second rows show the results where all joints of the robotic arm can freely rotate; the third and fourth rows contain the results where θ_1 and θ_2 are locked. According to Table II, the condition number of the effective mass matrix of the rigid RIM is always considerably larger than that of the flexible RIM for the same configuration. It can also be seen that the difference is more significant when the robotic arm is in a near-singular configuration as posture C. On the other hand, when two of the joints are locked, the condition numbers for the rigid RIM become very large in all configurations due to the reduced mobility of the system. For the same cases, the condition numbers for the flexible RIM still remain in a reasonable range. These conclusions based on the condition number are consistent with the analysis of the effective mass ellipsoids, showing that flexible RIM has a better-conditioned mass matrix and can prevent potential singularity and numerical problems that can be observed for the rigid RIM.

B. Simulation results

To demonstrate the stability of RIM-based co-simulation for flexible systems, and to show the difference between the rigid and flexible RIMs in simulation, a robotic contact task is implemented in MATLAB. Two similar manoeuvres of the robotic arm numbered 1 and 2 are designed to demonstrate the simulation and to compare the performance as shown in Fig. 6.

Manoeuvre 1 in Fig. 6a can be described as the following steps.

Step 1: From $t = 0$ to $t = 2s$, the robotic arm starts at Configuration D in Fig. 6a and slightly stretching the elbow to deliver the wrist along with the end-effector to the right side. At the same time, the wrist rotates to change the orientation

IEEE Robotics and Automation Letters (RA-L) paper, presented at ICRA 2024, Yokohama, Japan. Cite as RA-L paper.

IEEE Robotics and Automation Letters (RA-L) paper, presented at ICRA 2024, Yokohama, Japan. Cite as RA-L paper.

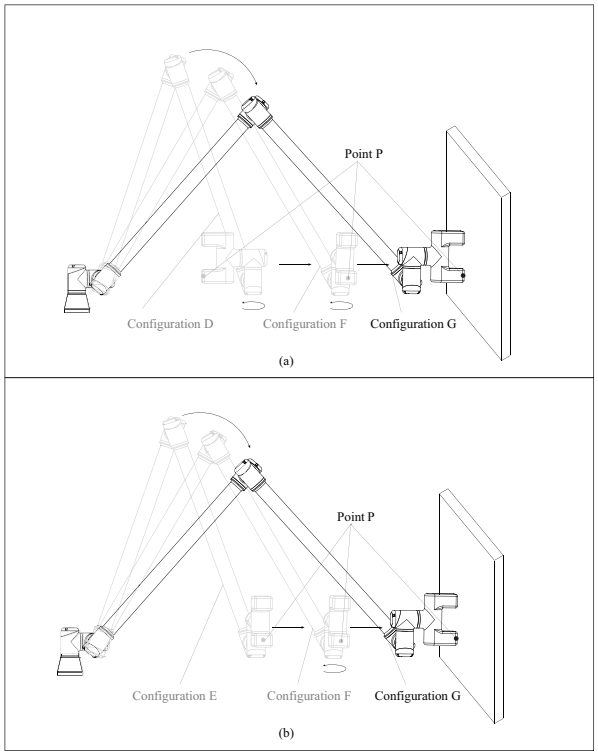

Fig. 6. (a) Designed Manoeuvre 1 for the robotic arm. (b) Designed Manoeuvre 2 for the robotic arm.

of the end-effector. The robotic arm reaches Configuration F and stays at this position for $0.5s$.

Step 2: The robotic arm continues stretching the elbow and rotating the wrist from $t = 2.5s$ to $t = 4.5s$ until it reaches Configuration G where the grasper is at the surface of the static wall. Then it stays for $0.5s$.

Step 3: After $t = 5s$, the end-effector is pushed against the static wall and contacts are established in the end-effector subsystem.

Manoeuvre 2 shown in Fig. 6b is similar to Manoeuvre 1. However, it starts at Configuration E, where the end-effector has the same orientation as in Configuration F. From $t = 0$ to $t = 2s$, the wrist of the robotic arm does not rotate and the end-effector undergoes a pure translation to the right side. When the robotic arm reaches Configuration F, it also stays for $0.5s$ and then follows the same motion as Steps 2 and 3 in Fig. 6a.

For both Manoeuvre 1 and 2, the second joint at the shoulder is locked starting from $t = 1.5s$, hence keeping θ_2 unchanged and reducing the degrees of freedom of the robotic arm. In this way, near-singular configurations are created during the manoeuvres. Note that the robotic arm passes by a near-singular Configuration F in Manoeuvre 1, while it remains at near-singular positions from $t = 1.5s$ to $t = 2.5s$ in Manoeuvre 2. Such a singular configuration of the robotic arm can occur in practice according to the singularity analysis [18].

The macro time step of co-simulation is $1/60\,s$. The robotic arm subsystem is simulated with a micro time step of $1/600\,s$ while the end-effector subsystem is numerically integrated every $1/120\,s$. Note that the selected time step size is in general too large for signal-based co-simulation and can cause instability, but the RIM-based approach performs more stably and allows for such time step size.

For this example, the simulation of the flexible model has comparable computational time to the rigid model. To compare the accuracy of simulation, the results of the RIM-based co-simulation for both the rigid and flexible systems are shown in Fig. 7. While a monolithic solution can be difficult in general cases, it is achieved in this example and is provided as a reference solution for both rigid and flexible models to determine the accuracy of the co-simulation. Fig. 7a shows the distance between Point P and the static wall during the simulation. The distance decreases as the grasper moves and rotates to the right side. It stays at a constant value when the motion pauses between $t = 2s$ and $t = 2.5s$. After $t = 4.5s$, Point P stays at the surface of the wall and can have contact against the wall, as indicated by the close-to-zero value of the distance. As Fig. 7a shows, the RIM-based co-simulation of both rigid and flexible models gives stable and accurate results compared to the reference solution for Manoeuvre 1.

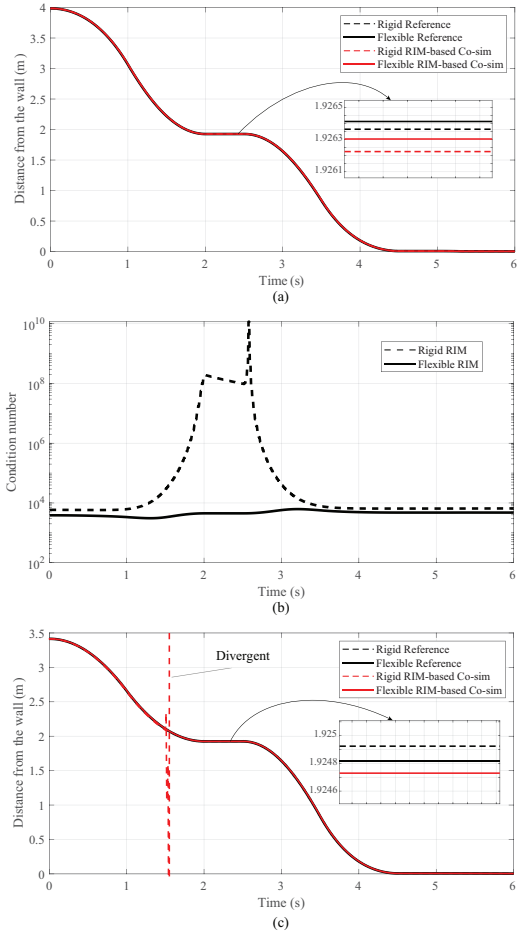

Fig. 7. Simulation results of (a) distance between Point P and the wall in Manoeuvre 1, (b) condition number of the effective mass matrix of RIMs in Manoeuvre 1, (c) distance between Point P and the wall in Manoeuvre 2.

However, the rigid RIM-based coupling leads to an ill-conditioned effective mass matrix during Manoeuvre 1, which is indicated by the condition number as in Fig. 7b. Since θ_2

IEEE Robotics and Automation Letters (RA-L) paper, presented at ICRA 2024, Yokohama, Japan. Cite as RA-L paper.

is fixed in the simulation, the Configuration F in Fig. 6a leads to a near-singular effective mass matrix in the rigid model. Therefore, during $t = 2s$ to $t = 2.5s$, the condition number of the effective mass for rigid RIM reaches very large values. On the contrary, the condition number of the flexible RIM stays in a reasonable range during the entire simulation. This means the rigid RIM-based co-simulation is prone to numerical errors in this case, and it can be avoided by including flexibility in the model.

This numerical problem for rigid RIM is observed more clearly from the simulation results of Manoeuvre 2 as shown in Fig. 7c, where the robotic arm stays at a near-singular position for a period of time. In this case, the rigid RIM-based coupling works well from $t = 0$ to $t = 1.5s$ when no joints are locked. But, it fails rapidly after the joint angle θ_2 is locked at $t = 1.5s$ because the effective mass matrix becomes ill-conditioned and loses important characteristics such as being positive definite. The simulation based on rigid RIM coupling thus can no longer provide physically meaningful results, as indicated by the divergent curve in Fig. 7c. On the other hand, the flexible RIM-based co-simulation still works for this challenging case and provides accurate results as compared to the reference solutions in Fig. 7c. The simulation results are consistent with the analysis of the effective mass matrices mentioned in the previous section.

This robotic example demonstrates the performance and advantages of co-simulation based on flexible RIM. The flexible RIM concept is general and can also be used for other cases with large deformations and multiple subsystems.

V. Conclusions

In this paper, we introduce a model-based co-simulation scheme for general mechanical systems with flexibility, in which *reduced interface models* (RIMs) are created to represent the dynamics of subsystems in terms of their interface behaviour. Here we introduced the flexible RIM formulation of robotic systems with structural flexibility and extended the formulation for constrained subsystems. Unlike the previous studies which are limited to rigid multibody systems, the flexible RIM formulation has broader applications.

A robotic arm model connected with another subsystem involving contacts is used as an example to demonstrate the RIM-based co-simulation and to compare the difference between the rigid and flexible RIMs. The robotic arm is modelled in two ways, with and without considering flexibility. The properties of the RIMs of these two models are compared based on the analysis of the effective mass matrices, showing that the flexible RIM has a better-conditioned mass matrix than the rigid RIM. To further confirm the conclusions, two maneouvres of contact tasks are designed and compared for the rigid and flexible models. The flexible RIM-based co-simulation preserves accurate results in cases where the rigid RIM leads to large errors.

The simulation results and analysis show a twofold conclusion: the RIM-based coupling approach can provide stable and accurate performance of co-simulation for robotic systems with flexibility, and flexible RIM can resolve the conditioning problems observed for robotic arm models where structural flexibility is not taken into account.

Acknowledgements

This work was supported by the Natural Sciences and Engineering Research Council of Canada (NSERC) and CM Labs Simulations Inc. Ali Raoofian was also supported by the Fonds de Recherche du Québec – Nature et Technologies (FRQNT), Canada. The support is gratefully acknowledged.

References

[1] J.-C. Samin, O. Brüls, J.-F. Collard, L. Sass, and P. Fisette, "Multiphysics modeling and optimization of mechatronic multibody systems," *Multibody System Dynamics*, vol. 18, no. 3, pp. 345–373, 2007.

[2] M. A. Naya, J. Cuadrado, D. Dopico, and U. Lugris, "An efficient unified method for the combined simulation of multibody and hydraulic dynamics: comparison with simplified and co-integration approaches," *Archive of Mechanical Engineering*, pp. 223–243, 2011.

[3] A. Peiret, F. González, J. Kövecses, and M. Teichmann, "Multibody system dynamics interface modelling for stable multirate co-simulation of multiphysics systems," *Mechanism and Machine Theory*, vol. 127, pp. 52–72, 2018.

[4] M. Arnold, B. Burgermeister, C. Führer, G. Hippmann, and G. Rill, "Numerical methods in vehicle system dynamics: state of the art and current developments," *Vehicle System Dynamics*, vol. 49, no. 7, pp. 1159–1207, 2011.

[5] C. Andersson, "Methods and tools for co-simulation of dynamic systems with the functional mock-up interface," Ph.D. dissertation, Lund University, 2016.

[6] R. Kübler and W. Schiehlen, "Modular simulation in multibody system dynamics," *Multibody System Dynamics*, vol. 4, no. 2, pp. 107–127, 2000.

[7] A. Peiret, F. González, J. Kövecses, and M. Teichmann, "Co-simulation of multibody systems with contact using reduced interface models," *Journal of Computational and Nonlinear Dynamics*, vol. 15, no. 4, p. 041001, 2020.

[8] T. Haid, G. Stettinger, D. Watzenig, and M. Benedikt, "A model-based corrector approach for explicit co-simulation using subspace identification," in *Proceedings of the Fifth Joint International Conference on Multibody System Dynamics*. Lisbon, Portugal, 2018, pp. 1–18.

[9] T. Haid, D. Watzenig, and G. Stettinger, "Analysis of the model-based corrector approach for explicit cosimulation," *Multibody System Dynamics*, pp. 1–27, 2022.

[10] I. Sharf and G. M. D'Eleuterio, "Parallel simulation dynamics for elastic multibody chains," in *Proceedings., IEEE International Conference on Robotics and Automation*. IEEE, 1990, pp. 740–746.

[11] J. Wang, Z.-D. Ma, and G. M. Hulbert, "A gluing algorithm for distributed simulation of multibody systems," *Nonlinear dynamics*, vol. 34, no. 1, pp. 159–188, 2003.

[12] P. Zhou, H. Ren, and P. Masarati, "A relaxed coupling method for algebraically constrained mechanical systems," *Multibody System Dynamics*, pp. 1–25, 2022.

[13] A. Raoofian, A. Peiret, J. Kövecses, and M. Teichmann, "Non-smooth unilateral reduced models for co-simulation of mechanical systems," *Mechanism and Machine Theory*, vol. 173, p. 104829, 2022.

[14] A. Peiret, F. González, J. Kövecses, M. Teichmann, and A. Enzenhoefer, "Model-based coupling for co-simulation of robotic contact tasks," *IEEE Robotics and Automation Letters*, vol. 5, no. 4, pp. 5756–5763, 2020.

[15] A. A. Shabana, *Dynamics of multibody systems*. Cambridge university press, 2020.

[16] J. J. Júdice, "Algorithms for linear complementarity problems," *Algorithms for Continuous Optimization: The State of the Art*, pp. 435–474, 1994.

[17] J. Kövecses and L. L. Kovács, "Inertia properties and representations in mechanical systems," in *International Design Engineering Technical Conferences and Computers and Information in Engineering Conference*, vol. 57168. American Society of Mechanical Engineers, 2015.

[18] S. B. Nokleby, "Singularity analysis of the canadarm2," *Mechanism and Machine Theory*, vol. 42, no. 4, pp. 442–454, 2007.